sciendo

*Green Sciences, 27, **4**, 46—57, 10.2478/pjct-2025-0020*

Molecular Dynamics Investigation of Interfacial Interactions and Wettability in Coal–SiO_2–Water Three-Phase Systems

Hanlin Chen

School of Architectural Engineering, Chongqing Industry Polytechnic University, Chongqing, 401120 China
**Corresponding author:* e-mail: chenhl@cqipu.edu.cn

Molecular dynamics simulations were conducted to examine how methylated and hydroxylated coal molecules interact with SiO_2 surfaces bearing corresponding functional groups. Coal adsorption and wetting strongly depended on both coal functional groups and substrate chemistry. Methylated coal (coalCH_3) formed dense, planar clusters on hydrophobic SiO_2–CH_3, achieving nearly complete surface coverage (contact angles: 58.5°–67.7° at the surface; 81.9°–94.4° at the tetrahedral bottom), whereas on hydrophilic SiO_2–OH it formed sparse spherical or rod-like aggregates (surface: 88.4°–130.6°; bottom: 64.4°–114.4°), indicating poor wettability. Hydroxylated coal (coalOH) exhibited chain-like clusters on SiO_2–CH_3 evolving into continuous adsorption layers, while on SiO_2–OH it formed interconnected strip-like structures with limited spreading (surface: 62.7°–113.2°; bottom: 69.9°–71°). The energy decomposition results indicated that the interaction in coalCH_3 systems is primarily governed by van der Waals forces, whereas electrostatic contributions play a dominant role in stabilizing coalOH structures, highlighting the influence of surface functionalization on adsorption and wetting behaviors.

Keywords: Coal functionalization; SiO_2 surface chemistry; Molecular dynamics simulation; Wetting behavior; Interfacial interactions.

Received: 10 September 2025; Accepted: 14 November 2025; Available online: 14.01.2026.

INTRODUCTION

Coalbed methane (CBM), a representative form of unconventional natural gas derived mainly from coal seams, has become an important contributor to clean energy development and the reduction of greenhouse gas emissions. The extraction efficiency of CBM largely depends on the interfacial interactions among coal, water, and gas phases within the coal seam. In natural coal reservoirs, water commonly occupies the pores and adheres to the coal surface, competing with methane for adsorption sites[1–2], so coal surface wettability directly affects fluid distribution, gas movement, and desorption, thereby impacting methane recovery efficiency. In addition to the intrinsic properties of coal, inorganic minerals such as quartz (SiO_2) significantly influence interfacial characteristics[4–5], altering local wettability and fluid–solid interactions. These effects are particularly important in hydraulic fracturing and CO_2-enhanced CBM recovery, where water and injected gases simultaneously interact with coal and mineral surfaces. Despite its importance, the microscopic mechanisms governing the wettability of coal–SiO_2–water systems remain poorly understood due to the complexity of the heterogeneous interface[6–7].

In recent years, extensive research combining molecular dynamics (MD) simulations with experimental analyses has been devoted to understanding the interfacial and wetting characteristics of coal, water, and mineral systems. Through molecular dynamics (MD) simulations, Zhao et al. comprehensively analyzed the effects of droplet configuration and coal surface topology on interfacial wettability, offering theoretical guidance for enhancing the precision and robustness of coal–water interfacial models toward sustainable coal use[8]. Sun et al.employed long-timescale MD simulations to study the quartz–water–supercritical CO_2 system. They revealed the molecular-level mechanisms of fluid distribution and capillary behavior on quartz surfaces, providing valuable insights into the interfacial phenomena occurring during CO_2-enhanced coalbed methane (CO_2-ECBM) recovery[2]. Similarly, Liu et al. developed and validated a generalized surface modeling approach to accurately quantify quartz wettability, revealing how hydroxyl density, temperature, surfactants, and crude oil composition collectively influence wetting behavior[9].

In addition, several studies have focused on modifying coal wettability to improve fluid management. Hao et al. combined experiments and molecular simulations to reveal that nonionic–anionic surfactant mixtures form tighter adsorption layers on coal dust, significantly enhancing wettability and improving dust reduction performance[10]. Jiang et al. showed, using experiments and molecular dynamics simulations, that coal surface wettability depends on functional group composition, with polar oxygen-containing groups (–COOH, –OH) increasing hydrophilicity through hydrogen bonding, offering insights for coal–SiO_2–water interfaces[11].

Overall, these studies highlight the critical role of coal surface chemistry and surfactant interactions in regulating wettability and fluid behavior. By elucidating how adsorption layers and functional groups influence hydrophilicity, they provide a mechanistic understanding that can guide the design of more efficient strategies for dust suppression and fluid management. Such insights are particularly relevant for complex coal–mineral–fluid systems, offering a foundation for optimizing interfacial interactions in both experimental and simulation contexts[12–13].

Despite considerable progress in understanding coal wettability and surfactant interactions, several gaps remain. Most existing studies have focused either on coal–water systems or on simple coal–mineral interfaces, often neglecting the combined effects of coal, mineral particles, and water in realistic multiphase environments[14–17]. Moreover, while functional groups and surfactants have been studied, the microscopic mechanisms governing interfacial

interactions in coal–SiO_2–water three-phase systems are still not fully understood[18–19]. This lack of detailed molecular-level insight limits the ability to predict and control wettability and fluid behavior in practical applications, such as dust suppression, enhanced oil/gas recovery, or coal beneficiation[20–22]. Against this backdrop, the current work focuses on the coal–SiO_2–water three-phase system, specifically probing how surface functionalisation (–CH_3 vs –OH) influences interfacial interactions and wettability at molecular resolution. By building on the molecular--scale insight from prior reservoir research, our study aims to bridge the gap between microscopic interfacial phenomena and macroscopic reservoir damage/recovery behaviours.

MODELING STRATEGIES AND SIMULATION DETAILS

Modeling Strategies

All molecular dynamics (MD) simulations were performed using the GROMACS 5.0.7 software package. Following the approach reported in Ref.[23], two types of coal molecular models were constructed, representing methylated and hydroxylated modifications (Fig. 1a-b). Considering the structural diversity of SiO_2 surfaces, two types of substrates were also modeled: a hydrophobic surface functionalized with methyl groups and a hydrophilic surface functionalized with hydroxyl groups (Fig. 1c-d). These four models were then combined in pairs to build composite systems, aiming to investigate the adsorption and wettability behavior of different coal molecules on SiO_2 surfaces with distinct surface properties (Fig. 1e-h). Each system contained 200 coal molecules, after which water molecules were added to match the density of liquid water at 298 K and 1 atm. The simulation box measured 14.2 × 5.2 × 7.7 nm^3, with periodic boundary conditions in all directions.

Simulation details

The OPLS-AA force field was applied to describe the atomic interactions of coal molecules[24]. The interactions of water molecules were represented by the TIP4P force field[25], with molecular rigidity maintained through the SETTLE algorithm. The SiO_2 substrate was represented by the CHARMM27 force field[26]. Non-bonded interactions between different atom types were calculated using the Lorentz–Berthelot mixing rule, which is widely adopted for Lennard-Jones parameters in molecular dynamics studies. The Lennard-Jones distance parameter(σ) for each pair of particles i and j is determined according to Equation (1):

$$\sigma_{ij} = \frac{\sigma_i + \sigma_j}{2} \tag{1}$$

The Lennard-Jones potential energy parameter (ε) is determined according to Equation (2):

$$\varepsilon_{ij} = \sqrt{\varepsilon_i \cdot \varepsilon_j} \tag{2}$$

Non-bonded interactions at short range were cut off at 1.20 nm, whereas long-range electrostatic forces were computed using the Particle Mesh Ewald (PME) approach, which separates the total electrostatic energy into real-space, reciprocal-space, and self-interaction contributions, as described in Equation (3):

$$E_{\text{total}} = E_{\text{real}} + E_{\text{reciprocal}} + E_{\text{self}} \tag{3}$$

The real-space term is calculated according to Equation (4):

$$E_{\text{real}} = \frac{1}{2}\sum_{i \neq j} q_i\, q_j \frac{\operatorname{erfc}(\kappa r_{ij})}{r_{ij}} \tag{4}$$

The reciprocal-space term is calculated according to Equation (5):

$$E_{\text{reciprocal}} = \frac{1}{2V}\sum_{\mathbf{k}\neq 0} \frac{4\pi}{k^2} e^{-k^2/4\kappa^2} \left| \sum_j q_j\, e^{i\mathbf{k}\cdot\mathbf{r}_j} \right|^2 \tag{5}$$

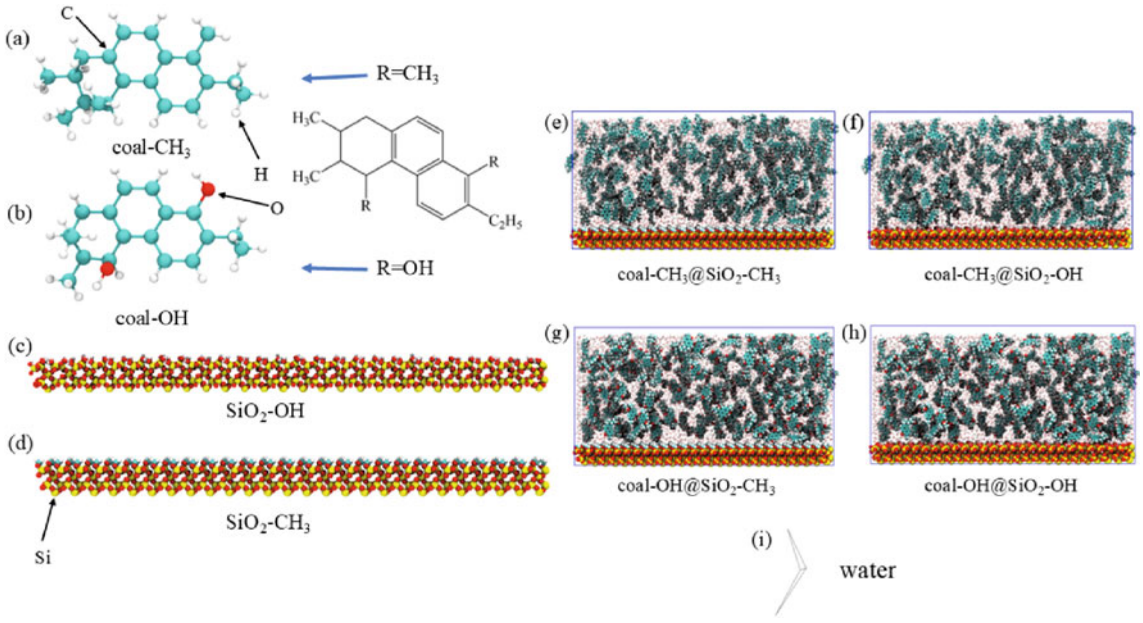

Figure 1. Coal molecules modified with (a)methyl/(b)hydroxyl groups; (c)hydroxyl/(d) Methyl-modified SiO_2; The initial structure of the composite system of methylated coal molecules and (e)methylated/(f)hydroxylated SiO_2; The initial structure of the composite system of hydroxylated coal molecules and (g)methylated/(h)hydroxylated SiO_2; (i) tip4p water model

The self-interaction term is calculated according to Equation (6):

$$E_{\text{self}} = -\frac{\kappa}{\sqrt{\pi}}\sum_{i} q_i^2 \tag{6}$$

In Equation (4), q_i denotes the charge of particle i, and r_{ij} represents the distance between particles i and j. The Ewald splitting factor, $\varkappa$, separates real-space and reciprocal-space contributions, while erfc stands for the complementary error function. V refers to the simulation cell volume, and k indicates the reciprocal-space wave vector.

The non-bonded interactions between atoms were modeled as the sum of Lennard–Jones (LJ) and electrostatic potentials, as described in Equation (7):

$$E_{\text{non-bonded}} = E_{\text{LJ}} + E_{\text{Coul}} \tag{7}$$

where the Lennard–Jones potential describes short-range van der Waals interactions as described in Equation (8):

$$E_{\text{LJ}}(r_{ij}) = 4\varepsilon_{ij}\left[\left(\frac{\sigma_{ij}}{r_{ij}}\right)^{12} - \left(\frac{\sigma_{ij}}{r_{ij}}\right)^{6}\right] \tag{8}$$

and the Coulombic potential accounts for electrostatic interactions, as described in Equation (9):

$$E_{\text{Coul}}(r_{ij}) = \frac{1}{4\pi\varepsilon_0}\frac{q_i q_j}{r_{ij}} \tag{9}$$

Here,r_{ij} is the distance between atoms i and j,ε_{ij} and σ_{ij} are the Lennard–Jones energy and size parameters, and q_i and q_j are the atomic partial charges. The initial configuration was subjected to energy minimization using the steepest descent algorithm to remove high-energy contacts. Afterwards, the system was equilibrated in the NPT ensemble at 350 K and 15 MPa for 2 ns, employing the V-rescale thermostat and Berendsen barostat with coupling times of 0.1 ps and 2 ps, respectively. A subsequent 20 ns NPT production run was carried out under the Nosé–Hoover thermostat and Parrinello–Rahman barostat to ensure accurate sampling of thermodynamic properties.

RESULTS AND DISCUSSION

Evolution of Coal Adsorption and Wetting Behavior on SiO_2 Surfaces

This study investigates the adsorption and wetting behavior of coal molecules bearing different functional groups on hydrophilic and hydrophobic SiO_2 surfaces. We monitored the structural evolution of four composite systems during a 20 ns molecular dynamics simulation. The representative morphologies of molecular arrangements at different time intervals were used to elucidate the interfacial interactions and wetting states. For the methylated coal molecules (denoted as coal–CH_3) adsorbed on the methylated SiO_2 surface (SiO_2–CH_3), a distinct aggregation pattern was observed (Fig. 2a). At 1 ns, coal–CH_3 molecules exhibited strong intermolecular attractions, rapidly forming cluster-like structures. These clusters preferentially adopted a planar configuration distributed at the upper boundary of the simulation box, while simultaneously forming a mountain-like protrusion on the SiO_2–CH_3 surface. As the simulation progressed, the loosely packed clusters dispersed in water gradually compacted and spread, eventually covering the entire SiO_2 surface. Meanwhile, the initial protrusion decreased in height, and a dense multilayer adsorption structure was established, indicating enhanced surface coverage and wetting. In contrast, coal–CH_3 molecules interacting with the hydroxylated SiO_2 surface (SiO_2–OH) exhibited a markedly different adsorption morphology (Fig. 2b). The top adsorption layer was relatively sparse and adopted a small-hill-like shape. On the SiO_2–OH surface itself, coal–CH_3 molecules tended to form three prominent clusters, which were mainly spherical or rod-like in shape. This morphology indicates poor wettability of coal–CH_3 on the hydrophilic surface. Interestingly, the rod-shaped cluster initially connected to the upper adsorption layer gradually detached during the simulation, splitting into two separate domains: one larger spherical cluster attached to the box top and another smaller one adsorbed directly on the SiO_2 surface. For hydroxylated coal molecules (coal–OH) on the hydrophobic SiO_2–CH_3 surface (Fig. 2c), a unique adsorption behavior was ob-

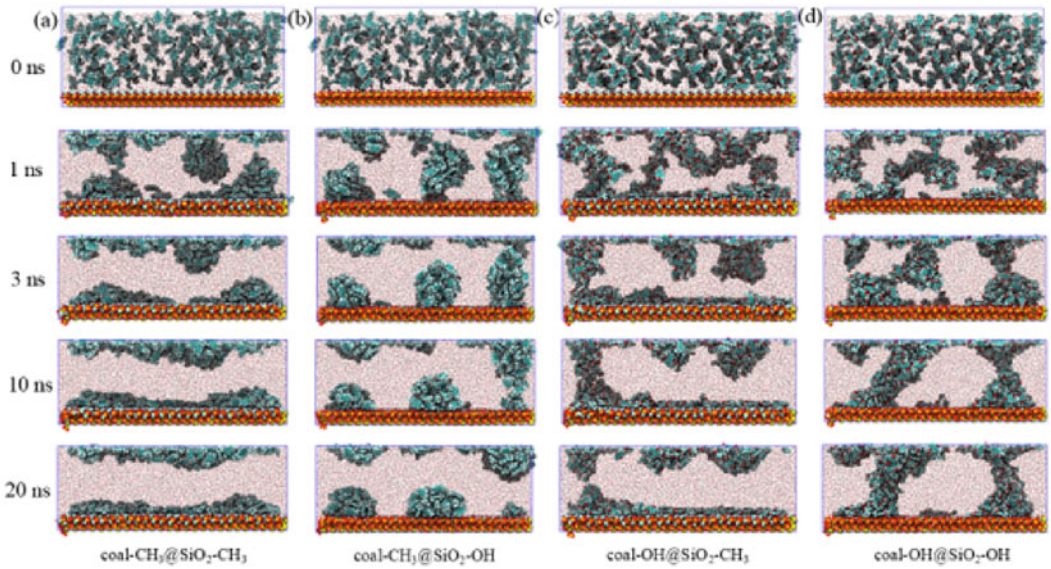

Figure 2. Adsorption Structural Evolution of Coal Molecules on SiO_2 Surfaces: (a, b) Methylated Coal on Methylated/Hydroxylated SiO_2; (c, d) Hydroxylated Coal on Methylated/Hydroxylated SiO_2

served. In the initial stage (1 ns), coal–OH molecules adopted elongated and intertwined chain-like clusters that extended across the simulation box. These clusters gradually fragmented into smaller substructures, adsorbing onto both the upper and lower interfaces. On the top surface, thin adsorption layers developed several spherical protrusions, reflecting limited wettability. By contrast, the coal–OH molecules on the SiO_2–CH_3 surface exhibited excellent wetting, spreading nearly uniformly and forming a continuous adsorption layer that almost completely covered the surface. Finally, for coal–OH molecules adsorbed on the hydroxylated SiO_2 surface (SiO_2–OH), the adsorption evolution shared similarities with the previous case in the early stage, characterized by irregular, interwoven block-like clusters (Fig. 2d). However, as the simulation advanced, coal–OH molecules located at the upper and lower interfaces gradually connected, forming a "molecular bridge" spanning across the system. Most coal–OH molecules were distributed along this bridge, while only a relatively thin adsorption layer remained on the SiO_2–OH surface. This configuration highlights the distinct wetting differences between coal molecules with various functional groups on hydrophilic and hydrophobic substrates. Structural compatibility and packing density between coal fragments and the SiO_2 surface also play a role in adsorption. The rigid and planar SiO_2 surface allows coal molecules to adopt orientations that maximize surface contact while minimizing steric hindrance, resulting in more efficient surface coverage. For methyl--functionalized surfaces, the spacing between functional groups accommodates the coal fragments without causing significant steric repulsion, further promoting dense packing. Together, these geometric considerations and polar interactions synergistically enhance the adsorption strength and stability of coal on the functionalized SiO_2 surfaces. This mechanistic insight highlights that both chemical interactions and physical compatibility contribute to interfacial behavior in coal–SiO_2 systems.

The evolution of the two-dimensional density cloud map of coal molecules over time

To provide a more intuitive understanding of the dynamic changes in coal molecular density and adsorption morphology, two-dimensional density contour maps were generated to illustrate the temporal evolution of coal molecule distributions in the four composite systems. Owing to the periodic boundary condition along the z-axis, coal molecules located at the top of the simulation box effectively correspond to adsorption on the bottom of the SiO_2 substrate, namely, the siloxane tetrahedral surface.

For the coal–CH_3@SiO_2–CH_3 system, coal molecules initially formed a prominent mountain-like structure on the SiO_2 surface, with density gradually decreasing outward from the interface (Fig. 3a). Between 3–10 ns (Fig. 3b), the protrusion became less pronounced, while the coal density near the SiO_2 surface and at the box bottom increased. During this stage, previously isolated clusters coalesced into a continuous adsorption domain. In the later stage (10–20 ns), the density distribution approached equilibrium, with coal–CH_3 exhibiting a significantly higher adsorption density on the siloxane tetrahedral surface compared to the methylated SiO_2 region (Fig. 3c). This observation suggests that methylated coal molecules preferentially adsorb onto the siloxane framework rather than the grafted methyl groups.

In the coal–CH_3@SiO_2–OH system, the coal molecules displayed a different adsorption pattern. At the hydroxylated SiO_2 surface, the density distribution was relatively sparse, with elongated strip-like structures extending outward and connecting with coal molecules adsorbed at the SiO_2 bottom surface (Fig. 3d). During the 3–10 ns interval (Fig. 3e), these elongated aggregates gradually fragmented, and the morphology transitioned into a small mountain-like configuration. Unlike the coal–CH_3@SiO_2–CH_3 case, the coal–CH_3 molecules here did not uniformly cover the entire SiO_2 surface. Instead, the density remained higher at the siloxane bottom surface than at the hydroxylated top surface, highlighting

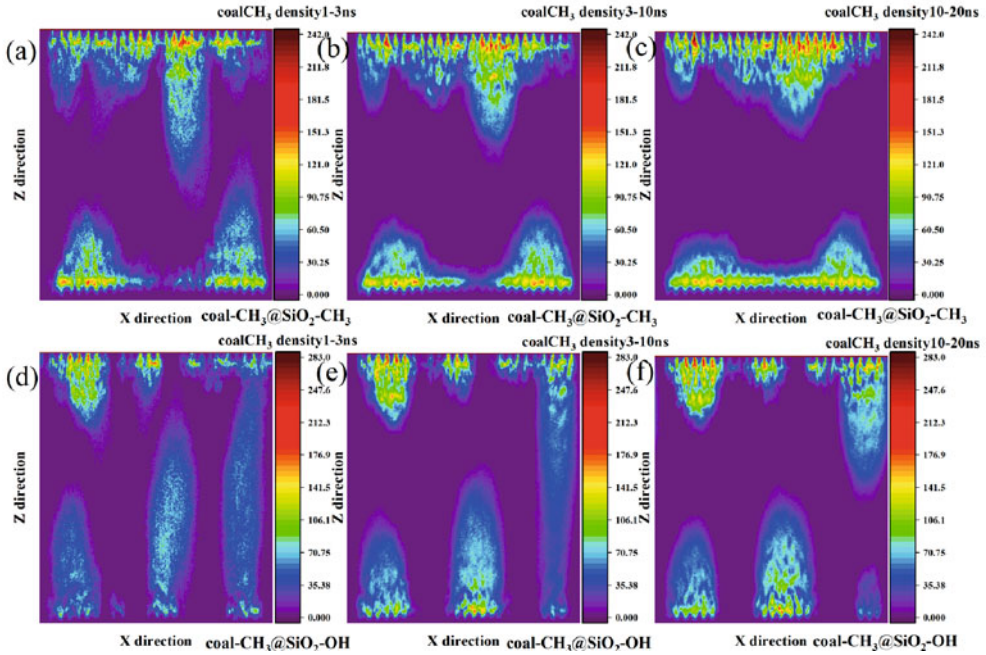

Figure 3. Average density cloud maps of coal-CH_3 in the coal-CH_3@SiO_2-CH_3 composite system within (a) 1–3 ns, (b) 3–10 ns and (c) 10–20 ns; Average density cloud maps of coal-CH_3 in the coal-CH_3@SiO_2-OH composite system within (d) 1–3 ns, (e) 3–10 ns and (f) 10–20 ns

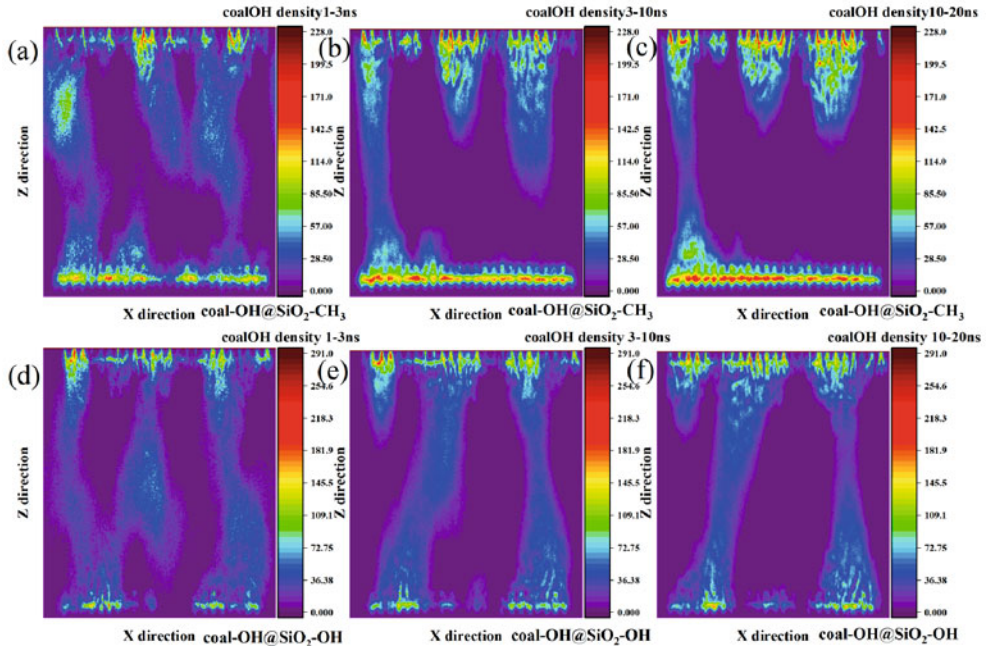

Figure 4. Average density cloud maps of coal-OH in the coal-OH@SiO_2-CH_3 composite system within (a) 1–3 ns, (b) 3–10 ns and (c) 10–20 ns; Average density cloud maps of coal-OH in the coal-OH@SiO2-OH composite system within (d) 1–3 ns, (e) 3-10 ns and (f) 10–20 ns

the poorer interfacial compatibility of methylated coal molecules with hydroxylated SiO_2 (Fig. 3e).

For the coalOH@SiO_2–CH_3 system, hydroxylated coal molecules exhibited good compatibility with the methylated SiO_2 surface. Within the first 1–3 ns (Fig. 4a), a continuous adsorption layer rapidly formed across the entire SiO_2 surface, with density increasing progressively closer to the substrate. In contrast, the density at the box top was less stable, appearing as scattered block-like clusters. During the 3–10 ns interval (Fig. 4b), these unstable blocks gradually contracted into mountain-like density protrusions, characterized by a gradual decay in density with increasing distance from the surface. From 10 to 20 ns (Fig. 4c), the two interfaces exhibited opposite density trends: a mountain-like aggregation of coal molecules formed on the siloxane tetrahedral surface, while on the methylated SiO_2 surface, coal–OH molecules spread evenly, resulting in a full adsorption layer.

In the coal–OH@SiO_2–OH system, the density distribution was less stable and displayed an interwoven morphology. Compared with the hydroxylated SiO_2 surface, the siloxane tetrahedral surface exhibited a higher coal density. Several thin and dispersed density domains initially appeared in the middle of the simulation box. Over time, these unstable domains fragmented, eventually leaving two elongated strip-like density regions that connected the upper and lower surfaces. This configuration suggests that hydroxylated coal molecules exhibit relatively weak wetting on hydroxylated SiO_2, preferring instead to form bridging structures that span across the system rather than uniformly adsorbing onto the substrate (Fig. 4d-f).

Radial distribution functions (RDFs) between coal molecules and other system components, along with the root mean square displacement (MSD) of coal molecules, were evaluated for the various composite systems

Radial distribution functions (RDFs) between selected atoms in coal molecules and terminal groups on the SiO_2

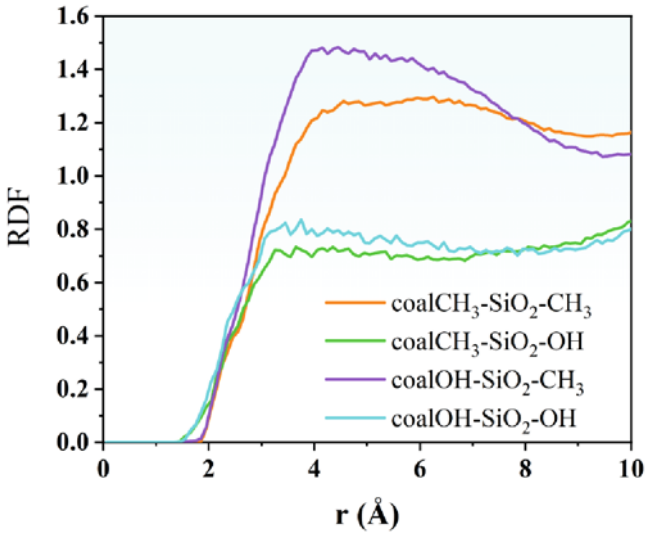

Figure 5. Radial distribution functions (RDFs) for interactions between methylated or hydroxylated coal molecules and methyl or hydroxyl groups on SiO_2 surfaces

surface reveal unique interfacial structures in the four composite systems (Fig. 5). Quantitatively, the strongest and most localized ordering is observed for hydroxylated coal on the methylated surface (coalOH @ SiO_2–CH_3): the RDF exhibits a prominent first peak at ~4.45 Å with a maximum g(r) ≈ 1.48, indicating a well-defined first coordination shell and relatively tight adsorption. By contrast, hydroxylated coal on the hydroxylated surface (coalOH @ SiO_2–OH) shows a smaller but clear first peak at ~3.75 Å with g(r) ≈ 0.84, consistent with moderate hydrogen-bond–driven contacts that are more distributed (less locally concentrated) than in the coalOH @ SiO_2–CH_3 case.

The methylated coal cases display qualitatively different features. For coalCH_3 @ SiO_2–CH_3, the dominant peak occurs at a substantially larger distance (~6.25 Å, g(r) ≈ 1.30) rather than at a short contact distance. This long-distance peak suggests layer-like or looser packing

(likely second-shell structuring or adsorption with larger separation), rather than a tightly bound first-shell coordination. The coalCH_3 @ SiO_2–OH profile shows no pronounced near-contact peak; it gradually rises toward ~10 Å with g(r) ≈ 0.83, indicating weak, non-specific interactions and the absence of a well-defined first solvation shell at short range.

Taken together, the RDF data indicate two key points: (1) hydroxyl functionalization on coal markedly increases local affinity to SiO_2, producing stronger, more localized structuring (highest g(r) and clear near-contact peaks); (2) methyl–methyl or methylated-coal interactions are substantially weaker and/or spatially more delocalized, producing either distant peaks (layering) or only weak long-range modulation. Mechanistically, the pronounced peak for coalOH @ SiO_2–CH_3 (4.45 Å, g(r)≈1.48) can be attributed to polar interactions and directional hydrogen bonding between coal –OH and surface oxygen/siloxane sites, whereas the methylated systems are dominated by dispersive (van der Waals) contacts and steric packing that do not produce a compact first coordination shell.

The observed differences among the RDF profiles can be fundamentally attributed to the intrinsic polarity and dynamic behavior of the coal functional groups. Hydroxylated coal molecules (–OH) exhibit strong directionality in their interactions with surface oxygen or silanol sites, forming short-range, well-defined coordination shells. This is manifested by the sharp RDF peak at ~4.45 Å (g(r) ≈ 1.48) in the coalOH @ SiO_2–CH_3 system, indicating localized adsorption driven by hydrogen bonding and polar attraction. By contrast, methylated coal (–CH_3) interacts mainly through van der Waals forces, leading to weaker and more spatially delocalized contacts. The resulting RDF peaks appear at larger separations or become gradually distributed, as in coalCH_3 @ SiO_2–OH, where g(r) ≈ 0.83. Furthermore, interfacial water modulates these behaviors by competing for hydrogen bonds on hydroxylated surfaces and being excluded from hydrophobic ones, thus shaping the degree of local structuring. Overall, the RDF variations reflect how the interplay of molecular polarity, interfacial hydrogen bonding, and surface wettability governs both the static arrangement and dynamic evolution of coal–SiO_2 interfaces.

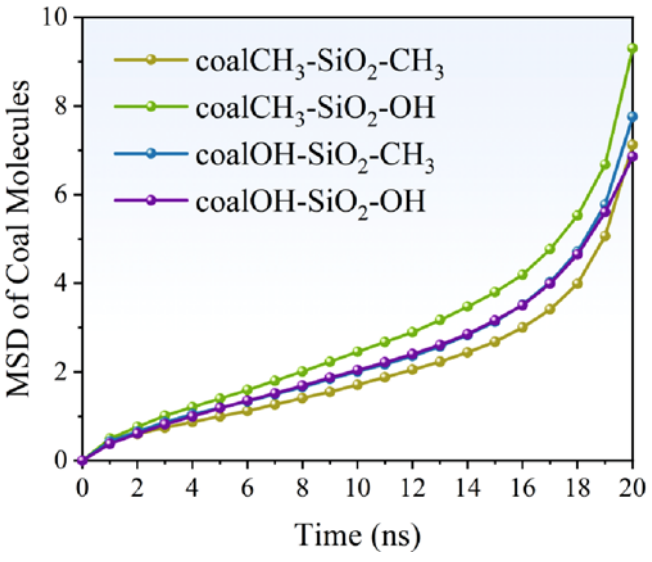

Figure 6. MSD of coal molecules in different composite systems

The time-dependent MSD curves of coal molecules in different SiO_2 composite systems reveal distinct diffusion behaviors (Fig. 6). At 20 ns, the MSD values for methylated coal in SiO_2–CH_3, methylated coal in SiO_2–OH, hydroxylated coal in SiO_2–CH_3, and hydroxylated coal in SiO_2–OH reached 7.12, 9.30, 7.76, and 6.86, respectively. For methylated coal, a pronounced difference was observed between the two surface types. The MSD in the SiO_2–OH system was approximately 31% higher than that in the SiO_2–CH_3 system, indicating that hydroxylated silica surfaces exert weaker adsorption constraints, thereby enhancing the translational mobility of methylated coal. In contrast, hydroxylated coal exhibited a different trend. The MSD in SiO_2–CH_3 was ~13% higher than in SiO_2–OH, reflecting stronger binding of hydroxylated coal on hydroxyl-rich surfaces due to hydrogen bonding, which significantly restricts its diffusion. Overall, methylated coal shows greater mobility than hydroxylated coal under identical conditions, suggesting that the substitution of hydroxyl groups in the coal molecule enhances surface affinity and suppresses translational dynamics. The results highlight the crucial role of surface chemistry in governing the behavior of coal molecules at the solid–liquid interface. Systems with reduced MSD of interfacial molecules display stronger surface interactions, leading to more stable adsorption layers and smaller contact angles, whereas systems with higher MSD show weaker interactions and larger contact angles. This relationship provides a mechanistic link between molecular dynamics and macroscopic wetting behavior.

The LJ and electrostatic interactions between coal molecules and other components

The temporal evolution of interaction energies between the methylated coal molecule and the SiO_2–CH_3 surface over 0–20 ns is presented in Fig. 7a. Van der Waals (Lennard–Jones, LJ) interactions are the primary contributors to the total energy, with values increasing from roughly –5600 kJ/mol at 0.5 ns to –10,600 kJ/mol at 20 ns. The LJ interaction gradually strengthens with simulation time, and a pronounced stabilization trend is observed after ~15 ns, where the energy fluctuates around –10,200 to –10,600 kJ/mol. This indicates the formation of a compact adsorption configuration, consistent with strong hydrophobic affinity between the methyl substituents of coal and the non-polar SiO_2–CH_3 groups. In contrast, the electrostatic interaction energy is relatively weaker, varying between –141 kJ/mol (0.5 ns) and –400 kJ/mol (19–20 ns). Although an order of magnitude smaller than the LJ term, the electrostatic contribution gradually increases over time and stabilizes around –350 to –400 kJ/mol after 10 ns. This enhancement reflects the partial contribution of induced dipole–dipole interactions and weak charge redistribution at the coal–surface interface, even in a nominally non-polar system.

For the coalCH_3@SiO_2–OH system (Fig. 7b), LJ interactions are the primary contributors during the adsorption process, decreasing from roughly –4201 kJ/mol at 0.5 ns to –7204 kJ/mol at 20 ns, which reflects a progressive enhancement of van der Waals forces as coal molecules align and pack on the hydroxylated surface. Although smaller in magnitude, the electrostatic contribution is significant, starting at –114 kJ/mol and

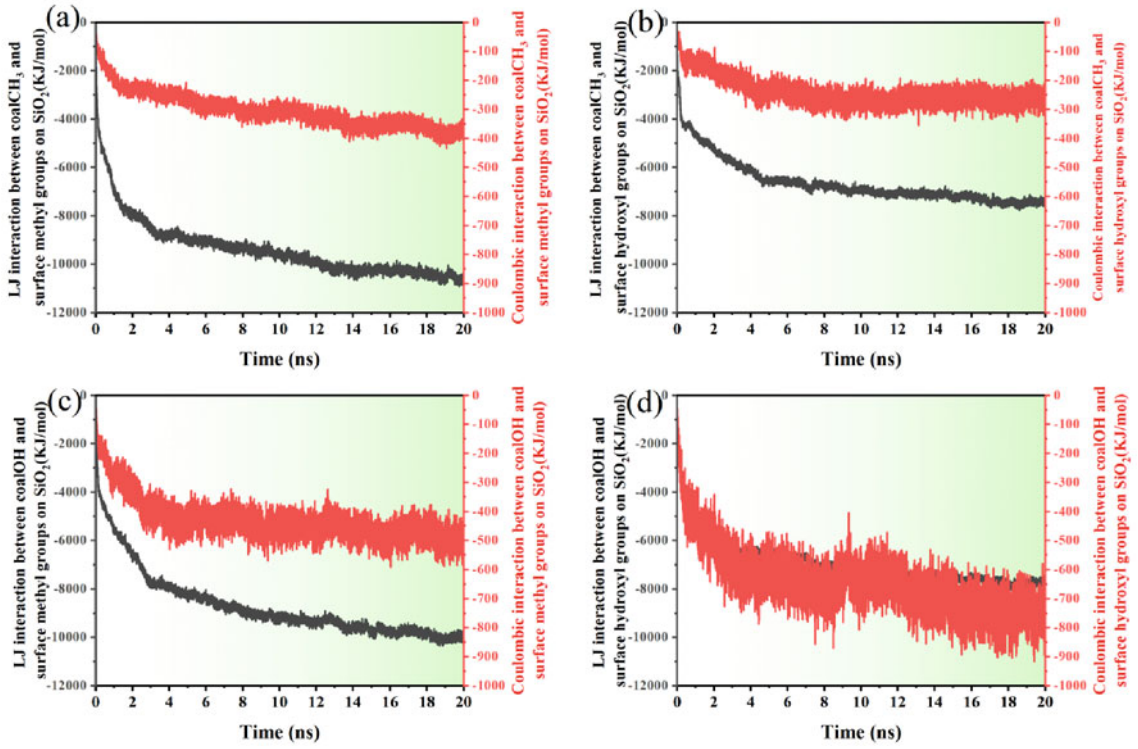

Figure 7. Time evolution of LJ and electrostatic interactions between coal molecules and surface functional groups: (a,.b) methylated coal with methyl/hydroxyl groups; (c,.d) hydroxylated coal with methyl/hydroxyl groups on SiO_2 surfaces

rising to –296 kJ/mol between 10 and 15 ns, suggesting the development of polar interactions and potential hydrogen bonds between coal –OH groups and the surface hydroxyl groups. In comparison, the coalCH_3@SiO_2–CH_3 system exhibits stronger LJ interactions overall, with initial values around –5591 kJ/mol at 0.5 ns decreasing to –10,600 kJ/mol at 20 ns, indicating more substantial van der Waals attraction due to favorable hydrophobic–hydrophobic contacts between methyl groups. However, the electrostatic contribution is significantly weaker, fluctuating around –141 kJ/mol initially and reaching –354 kJ/mol at 20 ns, which is considerably smaller than the peak values observed on the hydroxylated surface. This suggests that while hydrophobic interactions dominate on SiO_2–CH_3 surfaces, polar interactions are limited.

For the coalOH@SiO_2–CH_3 system (Fig. 7c), over the 20 ns simulation, the LJ interaction energy exhibits a consistently strong attractive trend, beginning at approximately −4568 kJ/mol at 0.5 ns and gradually decreasing to around −10022 kJ/mol at 20 ns. A progressive increase in LJ energy magnitude suggests that coal molecules become increasingly stabilized on the SiO_2–CH_3 surface, with van der Waals forces dominating the adsorption process. Notably, significant fluctuations in the LJ energy, for instance between 7–10 ns (from −8665 to −9324 kJ/mol), correspond to structural rearrangements of the coal molecules as they adapt to maximize contact with the surface. The electrostatic interaction, while considerably weaker than the LJ component, also shows a clear trend toward stronger attraction over time. The energy starts at –160 kJ/mol at 0.5 ns, decreases to a minimum of –551 kJ/mol at 16 ns, and then slightly fluctuates toward –494 kJ/mol by the end of the simulation. This trend highlights the role of hydroxyl groups on coal molecules interacting with surface dipoles or polarizable sites on methylated SiO_2. Although the electrostatic contribution is secondary to the van der Waals forces, its gradual strengthening indicates an increasing ordering of the hydrogen bonding network and local dipole alignment. When compared to the coalCH_3@SiO_2–CH_3 system, the coalOH@SiO_2–CH_3 interactions display slightly stronger LJ energies on average, reflecting the additional polar interactions contributed by the hydroxyl groups. Conversely, the electrostatic energies are also more pronounced than in the methylated coal case, highlighting the role of hydrogen-bonding potential in enhancing overall adsorption affinity.

The interaction energies between hydroxylated coal molecules and hydroxylated SiO_2 surfaces were also analyzed over a 20 ns molecular dynamics simulation to characterize adsorption behavior (Fig. 7d). The van der Waals (Lennard-Jones, LJ) interaction exhibited a generally increasing magnitude throughout the simulation, starting from −4826.9 kJ/mol at 0.5 ns and reaching −7598.7 kJ/mol at 20 ns. The gradual increase in LJ interactions indicates the development and stabilization of a dense adsorption layer on the surface. The LJ energy showed several minor fluctuations, for instance, a slight decrease at ∼4.0–5.0 ns and 6.5 ns, which may correspond to transient rearrangements of coal molecules during surface coverage. After approximately 7 ns, the LJ interactions stabilized between –7100 and –7800 kJ/mol, reflecting a steady adsorption configuration. Electrostatic interactions, mainly arising from hydrogen bonding and dipole–dipole contacts between coal hydroxyl groups and the surface, were much stronger than in nonpolar systems, with values changing from –342.3 kJ/mol at 0.5 ns to –795.9 kJ/mol at 20 ns. Several peaks were observed, including a prominent maximum of −824.7 kJ/mol at ∼17.5 ns and −785.1 kJ/mol at ∼13.0 ns, which can be attributed to optimal alignment of hydroxyl groups facilitating strong hydrogen bonding networks. Minor fluctuations throughout the trajectory suggest ongoing molecular rearrangements and dynamic interactions,

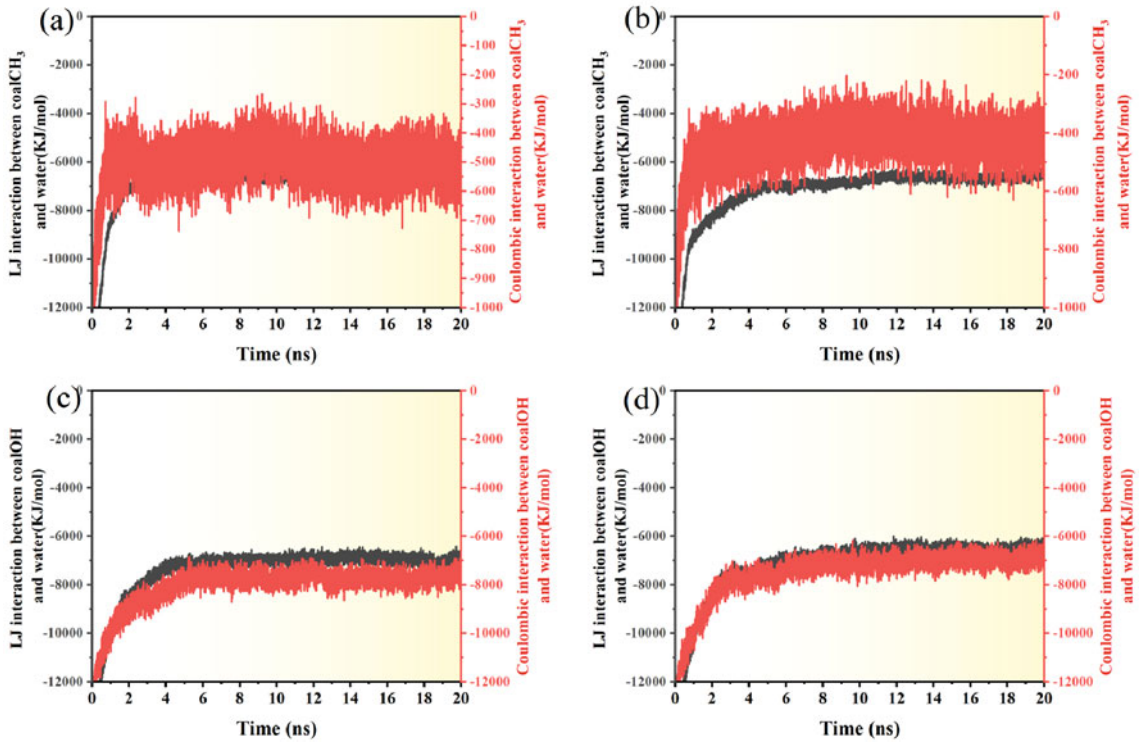

Figure 8. LJ and electrostatic interactions between coal molecules and water in different systems: (a, b) methylated coal with SiO_2–CH_3/SiO_2–OH; (c, d) hydroxylated coal with SiO_2–CH_3/SiO_2–OH

while the overall trend demonstrates progressively stronger electrostatic stabilization as the coal molecules increasingly interact with the SiO_2 surface.

Overall, the results indicate that both van der Waals and electrostatic interactions are important in coal adsorption on SiO_2, with electrostatic forces playing a significant role in stabilizing the adsorbed configuration. The time-dependent increase and stabilization of interaction energies signify the establishment of a well-ordered adsorption layer, consistent with efficient wetting by polar coal molecules.

Figure 8a illustrates the time-dependent LJ and electrostatic interactions between methylated coal molecules and water in the coalCH_3@SiO_2–CH_3 system over 20 ns. The LJ interaction exhibits large fluctuations throughout the simulation, with values ranging approximately from –11,100 kJ/mol at 0.5 ns to a minimum near –6,475 kJ/mol at 15 ns, suggesting a robust but dynamic van der Waals interaction between coal molecules and the surrounding water. Notably, the initial LJ interaction is the most negative (–11,110 kJ/mol), suggesting a highly favorable initial contact, which gradually relaxes as the system equilibrates and coal molecules adjust their configuration in the aqueous environment. The electrostatic interaction is consistently weaker in magnitude, fluctuating between –374 kJ/mol and –574 kJ/mol, reflecting moderate Coulombic contributions between coal functional groups and water molecules. The electrostatic energy exhibits smaller temporal variations compared to the LJ term, indicating relatively stable dipole–dipole interactions during the simulation. Peaks in the electrostatic interaction, such as around 3 ns (–513 kJ/mol) and 8 ns (–559 kJ/mol), correspond to transient structural rearrangements where polar groups of the coal molecules interact more closely with water molecules.

In the coalCH_3@SiO_2–OH system (Fig. 8b), the LJ interaction between methylated coal molecules and water exhibits an initial strong attraction of approximately –10,855 kJ/mol at 0.5 ns, followed by a gradual decrease with noticeable fluctuations, reaching –6,496 kJ/mol at 20 ns. This trend indicates that the van der Waals forces are initially dominated by close contacts between coal molecules and water molecules in the interfacial region, but gradually weaken as the system relaxes and the adsorption configuration stabilizes. The electrostatic interaction, initially –616 kJ/mol, exhibits moderate fluctuations throughout the simulation, ranging from –290 to –616 kJ/mol, highlighting the relatively weak polar interactions between coal's nonpolar methyl groups and water molecules. Notably, the LJ interaction is consistently larger in magnitude than the electrostatic contribution, suggesting that dispersion forces dominate the coal–water interaction in this system. Compared to the coalCH_3@SiO_2–CH_3 system, the overall LJ interaction in coalCH_3@SiO_2–OH is slightly weaker, with peak magnitudes around –10,855 kJ/mol versus –11,111 kJ/mol in the CH_3-modified silica system. Conversely, coalCH_3@SiO_2–OH exhibits slightly higher average electrostatic interactions, reflecting the enhanced polar contacts introduced by SiO_2 surface hydroxyl groups. These results indicate that while van der Waals interactions primarily drive the coal–water adsorption in both systems, the presence of surface hydroxyl groups slightly enhances electrostatic contributions, potentially facilitating a more heterogeneous interfacial interaction.

In the coalOH@SiO_2–CH_3 system (Fig. 8c), the Lennard-Jones (LJ) interaction between hydroxylated coal molecules and water is initially strong, reaching approximately $-1.23 \times 10_4$ kJ/mol at 0.5 ns. Within the first 5 ns, the LJ interaction gradually decreases to values around -7.1×10^3 to -8.1×10^3 kJ/mol, indicating

that the short-range van der Waals forces between coal and water stabilize after the initial contact. The electrostatic interaction shows a similar pattern, beginning around –1.07 × 10_4 kJ/mol and fluctuating between –7.2 × 10^3 and –8.3 × 10^3 kJ/mol, indicating stabilization of hydrogen bonds and polar contacts between coal hydroxyl groups and surrounding water. Both LJ and electrostatic interactions fluctuate over time but remain strongly negative, demonstrating that hydroxylated coal forms a stable adsorption layer with water even on the hydrophobic SiO_2–CH_3 surface. Notably, between 12–14 ns, a local increase in electrostatic interaction up to −8.2 × 10^3 kJ/mol corresponds to possible local rearrangement of water molecules or reinforcement of the hydrogen-bond network. The nearly equal contributions of LJ and electrostatic interactions suggest that coal–water interactions in this system are driven by both van der Waals forces and pronounced polar interactions.

For the coalOH@SiO_2–OH system (Fig. 8d), LJ and electrostatic interactions between hydroxylated coal molecules and water were analyzed throughout a 20 ns simulation. The LJ interaction fluctuates between approximately −11,805 and −6,370 kJ/mol, while the electrostatic interaction ranges from −10,620 to −6,839 kJ/mol. These results indicate a strong and persistent attractive interaction between the hydroxylated coal and water molecules, with both van der Waals and electrostatic contributions being substantial. Notably, the electrostatic component dominates the interaction energy throughout the simulation, highlighting the crucial role of hydrogen bonding and polar interactions in mediating water adsorption on the hydroxylated coal–SiO_2 surface. Temporal fluctuations are observed, reflecting dynamic rearrangements and transient water–coal contacts, yet the overall interactions remain highly favorable, suggesting robust coal–water affinity in this system.

A comparative analysis across all four coal–water systems (coalCH_3@SiO_2–CH_3, coalCH_3@SiO_2–OH, coalOH@SiO_2–CH_3, and coalOH@SiO_2–OH) reveals distinct interaction patterns. The LJ interactions in methylated coal systems (coalCH_3@SiO_2–CH_3 and coalCH_3@SiO_2–OH) generally exhibit weaker magnitudes (−6,500 to −11,000 kJ/mol) than those observed for hydroxylated coal systems (−6,500 to −12,300 kJ/mol), suggesting that the presence of surface hydroxyl groups enhances van der Waals attraction. Similarly, electrostatic interactions are significantly stronger in hydroxylated coal systems (up to −10,719 kJ/mol in coalOH@SiO_2–CH_3 and −10,620 kJ/mol in coalOH@SiO_2–OH) compared to methylated coal systems (approximately −574 to −616 kJ/mol), reflecting the pronounced hydrogen-bonding capability conferred by the –OH functional groups. Among all systems, coalOH@SiO_2–OH exhibits the most negative total interaction energy, indicating the strongest overall affinity between coal molecules and water, attributable to synergistic LJ and electrostatic contributions facilitated by dual hydroxylation on both the coal and SiO_2 surface.

Overall, coal functionalization and the surface chemistry of SiO_2 significantly affect coal–water interactions. Hydroxylated coal shows consistently stronger van der Waals and electrostatic interactions, while surface –OH groups on SiO_2 enhance water adsorption, highlighting the role of polar interactions in wetting and water-mediated transport in coal–mineral systems. The electrostatic component dominates near the hydrophilic SiO_2 surface, while the LJ term plays a more significant role in systems with organic modifiers. Moreover, the water density profiles reveal clear layering within the first two molecular layers adjacent to the surface, which slightly influences the local orientation of water molecules but has a negligible effect on the macroscopic contact angle.

Wetting behavior of coal molecules on the top and bottom surfaces of SiO_2

The interaction energies discussed in Section 3.4, including both Lennard–Jones and electrostatic contributions, govern the molecular adsorption and arrangement at the coal–SiO_2 interface. These energy interactions directly influence the stability and orientation of interfacial water molecules, which in turn determine the macroscopic wetting behavior and contact angles observed in the following analysis. For the coalCH_3@SiO_2–CH_3 system,

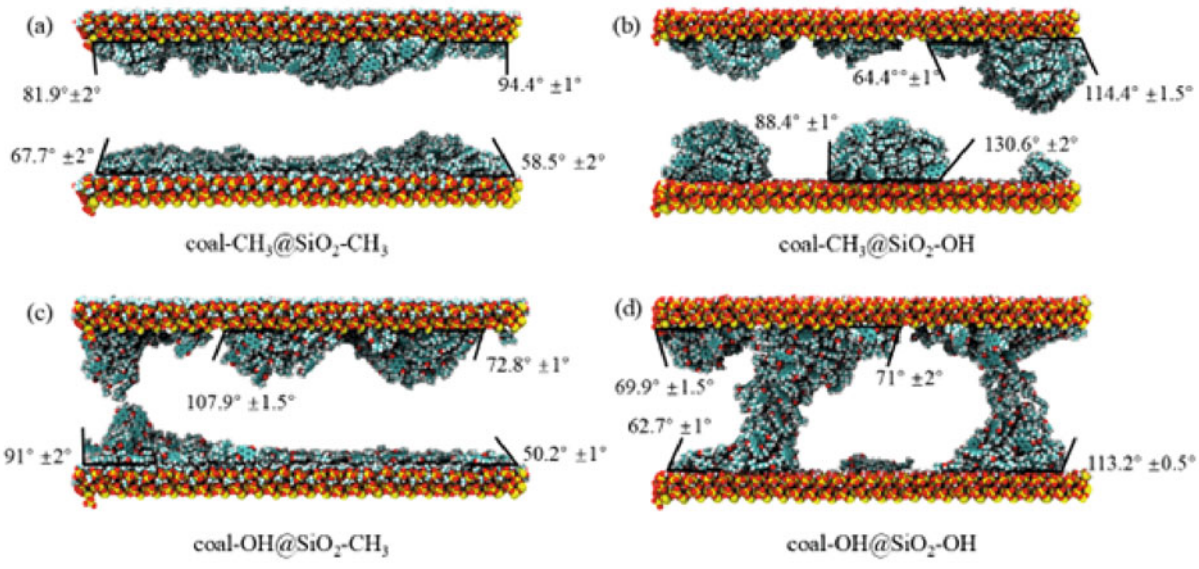

Figure 9. Wetting characteristics and contact angles of methylated coal molecules on the surface and bottom of (a)methylated/(b) hydroxylated SiO_2; The wetting characteristics and contact angles of hydroxylated coal molecules on the surface and bottom of (c)methylated/(d)hydroxylated SiO_2

the adsorption and wetting of methylated coal molecules on the SiO_2 surface and the underlying tetrahedral layer were examined (Fig. 9a). The contact angles were determined from the droplet profiles using a geometric fitting method, where the liquid–vapor interface was fitted to a circular arc, and the tangent angle at the intersection with the solid surface was taken as the contact angle. The results indicate that the methylated coal exhibits relatively good wettability across both regions, achieving near-complete contact with the substrate. Quantitatively, the contact angles measured on the SiO_2 surface range from 58.5° to 67.7°, suggesting a moderately hydrophilic interaction, whereas the contact angles on the underlying tetrahedral SiO_2 layer are slightly higher, ranging from 81.9° to 94.4°, indicative of reduced wetting affinity in this region. This discrepancy can be attributed to the relative exposure and chemical accessibility of surface functional groups, where the upper surface allows more favorable coal–substrate interactions, while the tetrahedral bottom imposes steric and geometric constraints that slightly hinder full spreading. Overall, these observations suggest that methylation of coal molecules promotes effective adsorption and partial spreading on both surface and subsurface SiO_2 regions, with the surface providing a more energetically favorable environment for wetting.

In the coalCH_3@SiO_2–OH system (Fig. 9b), methylated coal molecules exhibited weaker wetting on the hydroxylated SiO_2 surface and the underlying tetrahedral layer than on the methylated surface. The coal molecules exhibited poor wettability in both regions, often aggregating into multiple spherical clusters rather than spreading uniformly. Quantitatively, the contact angles on the hydroxylated surface ranged from 88.4° to 130.6°, indicating a predominantly hydrophobic behavior, while the contact angles on the tetrahedral bottom layer varied between 64.4° and 114.4°, reflecting considerable variability in wetting affinity due to local structural heterogeneity. These observations suggest that the presence of surface hydroxyl groups disrupts favorable coal–substrate interactions, promoting clustering and reducing the overall spreading ability of methylated coal molecules. These findings demonstrate that surface functionalization markedly affects coal wetting dynamics. Methylated coal exhibits weaker interactions with hydroxyl-rich SiO_2 surfaces, resulting in incomplete coverage and increased apparent contact angles.

In the coalOH@SiO_2–CH_3 system (Fig. 9c), the wetting behavior of hydroxylated coal molecules exhibited a pronounced spatial dependence between the methylated surface and the underlying tetrahedral layer. On the methylated surface, coal molecules displayed relatively good wettability, forming a continuous layer that effectively covered the substrate, with contact angles ranging from 50.2° to 91°. In contrast, at the tetrahedral bottom layer, the coal molecules exhibited poorer spreading, aggregating into multiple peak-like structures and resulting in higher contact angles between 72.8° and 107.9°. This disparity indicates that the local substrate topology and functionalization strongly influence coal wetting: the methylated surface promotes favorable coal–substrate interactions and uniform coverage, whereas the underlying tetrahedral layer limits spreading due to less accessible interaction sites and possible steric hindrance. Such anisotropic wetting behavior underscores the critical role of substrate surface chemistry and morphology in determining coal deposition and spreading patterns.

In the coalOH@SiO_2–OH system (Fig. 9d), the wetting behavior of hydroxylated coal molecules was generally poor on both the hydroxylated surface and the underlying tetrahedral layer. The coal molecules on both layers tended to aggregate and interconnect, forming elongated, strip-like structures rather than fully spreading over the substrate. The contact angles on the surface ranged from 62.7° to 113.2°, while those at the tetrahedral bottom were slightly more uniform, ranging from 69.9° to 71°. This morphology suggests limited coal–substrate interactions and stronger coal–coal cohesion, which hinder complete spreading. The formation of strip-like assemblies indicates that both surface functionalization and topography significantly influence the spatial distribution and wetting efficiency of coal molecules, with the hydroxylated substrate providing less favorable conditions for uniform coverage compared to methylated surfaces. Interfacial structuring and wetting behavior are sensitive to temperature and pressure. Higher temperatures generally increase molecular mobility, weaken hydrogen-bonding and van der Waals interactions, and may slightly increase contact angles, whereas higher pressures promote closer packing and stronger surface interactions, potentially reducing contact angles. These trends suggest that the observed interfacial properties could vary under different thermodynamic conditions, although the qualitative trends reported here are expected to remain robust.

In all simulated systems, the adsorption of coal molecules onto SiO_2 surfaces occurs through physisorption rather than chemisorption. The absence of any new covalent bond formation or charge transfer confirms that the observed interactions are governed by non-bonded forces, primarily van der Waals and electrostatic interactions. The hydroxylated coal molecules exhibit stronger and more localized adsorption due to hydrogen bonding with surface hydroxyl groups, whereas methylated coal interacts mainly through dispersion forces with hydrophobic SiO_2–CH_3 sites.

4. Conclusions

Molecular dynamics simulations were conducted to systematically explore how coal molecules with different functional groups interact with methylated and hydroxylated SiO_2 surfaces. Coal adsorption and wetting behaviors strongly depend on both coal functionalization and SiO_2 surface chemistry. Methylated coal (coal–CH_3) forms dense, planar clusters on hydrophobic SiO_2–CH_3, achieving nearly complete surface coverage, whereas on hydrophilic SiO_2–OH it assembles into sparse spherical or rod-like clusters, indicating poor wettability. Hydroxylated coal (coal–OH) exhibits chain-like clusters on SiO_2–CH_3 that evolve into a continuous adsorption layer, while on SiO_2–OH it forms interwoven block-like clusters and a "molecular bridge" connecting the top and bottom interfaces, leaving a thin layer on the surface. These results demonstrate that the interplay between coal functional groups and substrate hydrophilicity governs adsorption morphology and wetting characteristics.

Analysis of mean square displacement (MSD) revealed that hydroxylated coal molecules generally exhibited higher mobility than methylated coal, with the coalOH@

SiO_2–OH system showing the largest MSD values, indicative of weaker coal–substrate interactions and enhanced diffusion. Interfacial interactions were further elucidated through Lennard-Jones (LJ) and electrostatic energy analyses. For coal–SiO_2 interactions, methylated coal displayed stronger LJ interactions with SiO_2–CH_3 (~–10,600 kJ/mol) compared to SiO_2–OH (~–7,200 kJ/mol), while electrostatic contributions remained relatively minor (~–300 kJ/mol). Conversely, hydroxylated coal exhibited significantly stronger electrostatic interactions, particularly on SiO_2–OH (~–800 kJ/mol), highlighting the dominant role of hydrogen bonding and polar interactions. Coal–water interactions followed a similar trend: hydroxylated coal molecules interacted more strongly with water than methylated coal, with combined LJ and electrostatic interactions reaching –20,000 kJ/mol in coalOH@SiO_2–OH, emphasizing enhanced hydrophilicity induced by hydroxyl groups.

Wetting analyses and contact angle measurements provided further insight into the structural manifestations of these interactions. Methylated coal exhibited good wetting on SiO_2–CH_3, achieving nearly complete surface coverage with contact angles of 58.5°–67.7° on the surface and 81.9°–94.4° at the tetrahedral bottom. On hydroxylated surfaces, methylated coal formed spherical aggregates with larger contact angles (surface: 88.4°–130.6°; bottom: 64.4°–114.4°), reflecting poorer wetting. Hydroxylated coal showed heterogeneous wetting behavior: on SiO_2–CH_3, surface coverage was relatively complete (50.2°–91°) while bottom layers exhibited multiple peak-like clusters (72.8°–107.9°). On SiO_2–OH, hydroxylated coal formed interconnected strip-like structures with contact angles ranging 62.7°–113.2° on the surface and 69.9°–71° at the bottom, indicative of limited spreading and strong coal–coal cohesion.

Collectively, these results reveal that both coal functionalization and SiO_2 surface chemistry critically govern interfacial dynamics, interaction energies, and wetting behavior. Methyl groups favor dispersion on methylated substrates via van der Waals interactions, whereas hydroxyl groups enhance polar interactions and water affinity, leading to stronger electrostatic stabilization. The ability to tune coal surface chemistry provides a practical handle for industrial dust suppression strategies. Introducing polar functional groups can enhance water adhesion and wetting, improving dust capture efficiency, while hydrophobic modifications may be used to control moisture levels. These insights enable the rational design of additives and formulations tailored to specific operational needs in coal handling and processing industries

Author Contributions

H.C., Conceptualization, investigation, methodology, formal analysis, writing—original draft, funding acquisition, writing—review and editing. All authors have read and agreed to the published version of the manuscript.

Funding

This study was supported by Natural Science Foundation of Chongqing (Grant No. CSTB2025NSCQ--GPX0832), the Key Project of Chongqing Technology Innovation and Application Development (Grant No-.CSTB2025TIAD-KPX0028), the Guizhou Provincial Science and Technology Foundation (Grant No. Qian Ke He Zhi Cheng [2023] Yiban 482).

Data Availability Statement

The original contributions presented in this study are included in the article material. Further inquiries can be directed to the corresponding author.

LITERATURE CITED

1. Arif, M., Awan, F.U.R., Zhang, H. & Hosseini, M. (2024). Coal wettability: A holistic overview of the data sets, influencing factors, and knowledge gaps. *Energy Fuels*, 38(16), 15069–15084. DOI:10.1021/acs.energyfuels.4c03052.

2. Sun, E.W.H. & Bourg, I.C. (2020). Molecular dynamics simulations of mineral surface wettability by water versus CO_2: Thin films, contact angles, and capillary pressure in a silica nanopore. *J. Phys. Chem.* C, 124(46), 25382–25395. DOI:10.1021/acs.jpcc.0c07948.

3. Chen, C., Wan, J., Li, W. & Song, Y. (2015). Water contact angles on quartz surfaces under supercritical CO_2 sequestration conditions: Experimental and molecular dynamics simulation studies. *Int. J. Greenhouse Gas Control*, 42, 655–665. DOI: 10.1016/j.ijggc.2015.09.019.

4. Han, Q., Deng, C., Jin, Z. & Gao, T. (2021). Molecular simulation of the adsorption characteristics of methane in pores of coal with different metamorphic degrees. *Molecules*, 26(23), 7217. DOI: 10.3390/molecules26237217.

5. Jia, J., Song, H. & Jia, P. (2023). Molecular simulation of methane adsorption properties of coal samples with different coal rank superposition states. ACS omega, 8(3), 3461–3469. DOI: 10.1021/acsomega.2c07471.

6. Mwakipunda, G.C., Wang, Y., Mgimba, M.M., Ngata, M.R., Alhassan, J., Mkono, C. N. & Yu, L. (2023). Recent advances in carbon dioxide sequestration in deep unmineable coal seams using CO_2-ECBM technology: experimental studies, simulation, and field applications. *Energy Fuels*, 37(22), 17161–17186. DOI:10.1021/acs.energyfuels.3c03004.

7. Liu, H., Li, Z., Zheng, C., Wang, Y., Song, F. & Meng, X. (2023). Wettability characteristics of low-rank coals under the coupling effect of high mineralization and surfactants. ACS omega, 8(42), 39004–39013. DOI:10.1021/acsomega.3c03583.

8. Zhao, J., Lin, B., Lin, M., Liu, T., Liu, T. & Ma, S. (2025). New insights from molecular dynamic simulation on coal–water interface wettability. *Chem. Eng. Sci*., 122131. DOI:10.1016/j.ces.2025.122131.

9. Liu, B., Lei, X., Ahmadi, M., Jiang, L. & Chen, Z. (2024). Surface modeling of wettability transition on α-quartz: insights from experiments and molecular dynamics simulations. *J. Mol. Liq*., 406, 125147. DOI: 10.1016/j.molliq.2024.125147.

10. Hao, T., Jiang, S., Wang, L. & Jiang, W. (2024). Experimental and molecular dynamics simulation study of the effect of composite surfactants on wetting of coal dust. *J. Mol. Liq*., 409, 125552. DOI: 10.1016/j.molliq.2024.125552.

11. Jiang, B., Zhou, Y., Ji, B., Zheng, Y., Yu, C. F., Huang, J. & Wang, X. H. (2023). Investigation on the effect of functional groups on the wettability of coal dust: Experiments and theoretical validation. *Fuel,* 351, 128987. DOI: 10.1016/j.fuel.2023.128987.

12. Liu, Y.T., Li, H.M., Gao, M.Z., Ye, S.Q., Zhao, Y., Xie, J. & Zhou, W.Q. (2021). Experimental and molecular dynamics study into the surfactant effect upon coal wettability. *RSC Adv.,* 11(40), 24543–24555. DOI: 10.1039/D1RA01882E.

13. Xiao, P., Yang, X., Wang, R., Lin, H., Zhao, B., Liu, X. & Li, E. (2025). Investigating the interaction mechanisms of coal, water, and nano-SiO_2 modified by different amounts of SDBS via molecular simulation. *Surf. Interfaces*, 107229. DOI: 10.1016/j.surfin.2025.107229.

14. Wang, C., Yue, J., Zhang, M., Shi, B., Liang, Y. & Lou, Z. (2025). Wetting behavior and interaction mechanism between gas-containing coal and active water. Phys. *Fluids*, 37(8). DOI: 10.1063/5.0286685.

15. Si, L., Xi, Y., Wei, J., Liu, Y., Sheng, L. & Zhang, J. (2022). Solid-liquid contact characteristics and microscopic wetting mechanism between coal and water in gas atmosphere. *Fuel Process. Technol*., 236, 107403. DOI: 10.1016/j.fuproc.2022.107403.

16. Li, C., Zhang, J., Han, J. & Yao, B. (2021). A numerical solution to the effects of surface roughness on water–coal contact angle. *Sci. Rep*., 11(1), 459. DOI:10.1038/s41598-020-80729-9.

17. Gosiewska, A., Drelich, J., Laskowski, J.S. & Pawlik, M. (2002). Mineral matter distribution on coal surface and its effect on coal wettability. *J. Colloid Interf. Sci*., 247(1), 107–116. DOI: 10.1006/jcis.2001.8130.

18. Zhang, R., Xing, Y., Xia, Y., Luo, J., Tan, J., Rong, G. & Gui, X. (2020). New insight into surface wetting of coal with varying coalification degree: An experimental and molecular dynamics simulation study. *Appl. Surf. Sci.,* 511, 145610. DOI: 10.1016/j.apsusc.2020.145610.

19. Huang, Q., Yan, Y., Wang, G., Xie, J., Huang, Y., Li, M. & Feng, X. (2024). Imbibition behavior of water on coal surface and the impact of surfactant. *Fuel*, 355, 129475. DOI: 10.1016/j.fuel.2023.129475.

20. Li, M., Liu, J. & Xia, Y. (2025). Risk Prediction of Gas Hydrate Formation in the Wellbore and Subsea Gathering System of Deep-Water Turbidite Reservoirs: Case Analysis from the South China Sea. *Res. Sci.*, 1(1), 52–72. DOI: 10.62762/RS.2025.567907.

21. Wu, J. & Ansari, U. (2025). From CO_2 Sequestration to Hydrogen Storage: Further Utilization of Depleted Gas Reservoirs. *Res. Sci*. 1(1), 19–35. DOI: 10.62762/rs.2025.860510.

22. Barati, R. & Liang, J.T. (2025). Effects of Crosslinking Agents and Reservoir Conditions on the Propagation of Fractures in Coal Reservoirs During Hydraulic Fracturing. *Res. Sci*. 1(1), 36–51. DOI: 10.62762/RS.2025.494074.

23. Zhang, H., Song, C., Zhang, X., Zhao, H., Du, S., Tao, W. & Lv, Y. (2023). Synergistic effect of small molecular organic matter and functional groups in coal on methane adsorption. *ACS omega*, 9(1), 1156–1165. DOI: 10.1021/acsomega.3c07419.

24. Jorgensen, W. L., Maxwell, D.S. & Tirado-Rives, J. (1996). Development and testing of the OPLS all-atom force field on conformational energetics and properties of organic liquids. *J. Am. Chem. Soc*. 118(45), 11225–11236. DOI: 10.1021/ja9621760.

25. Jorgensen, W.L., Chandrasekhar, J., Madura, J.D., Impey, R.W. & Klein, M.L. (1983). Comparison of simple potential functions for simulating liquid water. *J. Chem. Phys*., 79(2), 926–935. DOI: 10.1063/1.445869.

26. MacKerell Jr, A.D., Banavali, N. & Foloppe, N. (2000). Development and current status of the CHARMM force field for nucleic acids. *Biopolymers*, 56(4), 257–265. DOI: 10.1002/1097-0282(2000)56:4<257::AID-BIP10029>3.0.CO;2-W.